

Physical and Magnetic Properties of Calcium-Substituted Li-Zn Ferrite

A.A. Sattar, H.M. El-Sayed, and W.R. Agami

(Submitted February 14, 2006)

The effect of Ca-substitution on the physical and magnetic properties of $\text{Li}_{0.3-0.5x}\text{Zn}_{0.4}\text{Ca}_x\text{Fe}_{2.3-0.5x}\text{O}_4$ ferrites ($x = 0.0, 0.01, 0.02, 0.03, \text{ and } 0.05$), prepared by the standard ceramic method, has been studied. It is found that the saturation magnetization increases up to $x = 0.01$ and then it decreases. On the other hand, the initial permeability decreased while the Curie temperature remained almost constant with increasing x . The coercivity and remanence ratio increased with increasing x .

Keywords coercivity, electrical resistivity, initial permeability, magnetization, remanence, X-ray diffraction

1. Introduction

Li-Zn ferrites are low-cost materials and have important properties for technological applications. It is known that the intrinsic parameters of ferrites, such as magnetization, initial permeability, Curie temperature, and resistivity depend on the chemical composition, heat treatment, and type of additive or substituted ions (Ref 1). The rectangularity of B-H loop is also found to increase with increasing the defects that hinder the magnetic domain wall motion in the grains (Ref 2). The influence of additives, such as Na_2O , CaO , Sb_2O_3 , and ZrO_2 on the structure, magnetic and electrical properties of Li-Zn ferrites were previously reported (Ref 1, 3). This paper is devoted to study the effect of Ca^{2+} substitution, not additives, on the physical and magnetic properties of Li-Zn ferrite.

2. Experimental Techniques

Ferrite samples with the chemical formula $\text{Li}_{0.3-0.5x}\text{Zn}_{0.4}\text{Ca}_x\text{Fe}_{2.3-0.5x}\text{O}_4$ ($x = 0.0, 0.01, 0.02, 0.03, \text{ and } 0.05$) were prepared by the standard ceramic method. High purity oxides, 99.99%, of ZnO and Fe_2O_3 with Li_2CO_3 and CaCO_3 were mixed together according to their molecular weight. The mixture of each sample was ground to a very fine powder and then presintered at 800°C for 6 h. The presintered mixture was ground again and pressed at room temperature, under a pressure

of 7×10^8 Pa, into tablet and toroidal forms. They were finally sintered at 1050°C for 3 h and then slowly cooled to room temperature. X-ray diffraction patterns were performed using a diffractometer of type X'Pert Graphics and identified with $\text{Cu } K_\alpha$ radiation. The theoretical x-ray density (d_x) of the samples was calculated using the formula ($d_x = 8M/Na^3$) where M is the molecular weight, N is Avogadro's number, and a is the lattice parameter. The density (d) of each composition was measured in bidistilled water using Archimedes' principle. The porosity percentage P (%) was calculated according to the relation $P = 100(1 - d/d_x)\%$. The magnetization (M), at room temperature, was measured using the vibrating sample technique. The magnetizing field ranged from 0.0 up to 1.4 T. A toroidal sample of each composition was used as a transformer core for measuring the initial permeability μ_i which was measured as a function of temperature at a constant frequency $f = 10$ KHz. The value of μ_i was calculated using Poltinnikov's formula (Ref 4), $V_s = K\mu_i$, where V_s is the induced voltage in the secondary coil and $K = \mu_0 n_p n_s I_p A \omega / L$; n_p and n_s are the number of turns of the primary and secondary coils, respectively, I_p is the current in the primary coil, A is the cross-sectional area of the sample, ω is the angular frequency, and L is the average path of the magnetic flux. Moreover, the coercive field and remanence were determined from the hysteresis loop. The tablet samples were used for the electrical resistivity measurements. The sample was inserted between two platinum electrodes where In-Hg was used as a contact material.

3. Results and Discussion

The x-ray diffraction patterns, (Fig. 1), showed that all investigated samples have single-cubic spinel phase. The d -spacing for each peak was recorded automatically and then the lattice parameter (a) was calculated from the relation

$$a = d_{hkl}(h^2 + k^2 + l^2)^{1/2}$$

The values of the lattice parameters obtained for each reflected plane are plotted against the function $F(\theta)$ where $F(\theta) = (1/2)[(\cos^2\theta/\sin\theta) + (\cos^2\theta/\theta)]$; θ is the Bragg's angle.

A. A. Sattar is on leave from Physics Department, Faculty of Science, Ain Shams University, Cairo, Egypt

A.A. Sattar and H.M. El-Sayed, Department of Basic Science, Faculty of Engineering, Misr University for Science and Technology, Cairo, Egypt; and W.R. Agami, Department of Physics, Faculty of Science, Ain Shams University, Cairo, Egypt. Contact e-mail: Adel_Sattar@maktoob.com.

Straight lines were obtained and the accurate values of (a) were determined from the extrapolation of these lines to $F(\theta) = 0$ (Ref 5). The variation of the lattice parameter (a) as a function of Ca-concentration (x) is shown in Fig. 2. It can be seen that the lattice parameter slightly increases linearly with the Ca-concentration, which obeys Vegard's law. Such an increase can be understood from the fact that we substitute Fe^{3+} and Li^{1+} ions by Ca^{2+} ion which has a larger ionic radius ($r_{\text{Fe}^{3+}} = 0.64 \text{ \AA}$, $r_{\text{Li}^{1+}} = 0.68 \text{ \AA}$, and $r_{\text{Ca}^{2+}} = 0.99 \text{ \AA}$). It is also noticed that the value of the lattice parameter (a) for the unsubstituted sample $\text{Li}_{0.3}\text{Zn}_{0.4}\text{Fe}_{2.3}\text{O}_4$ (8.3817 \AA) compares well with those reported earlier (8.378 \AA (Ref 1, 6), 8.380 \AA (Ref 3)).

4. Magnetic Studies

4.1 Magnetization

Figure 3 indicates the variation of magnetization M (emu/g) vs. the applied magnetic field $H(T)$ at the room temperature. As a normal behavior, the magnetization increases with increasing the applied magnetic field and attains its saturation value for

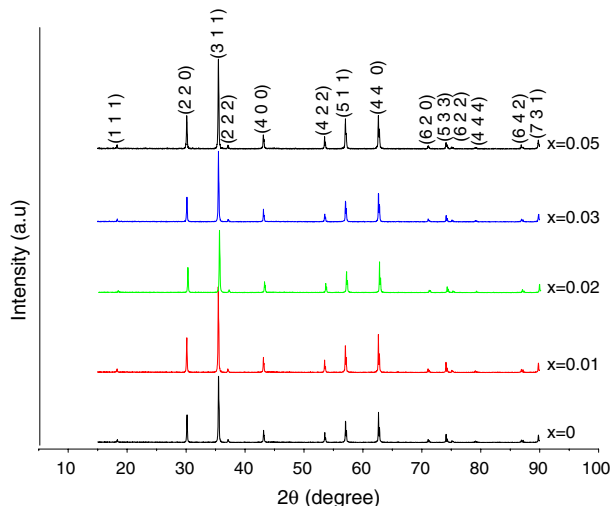


Fig. 1 X-ray diffraction patterns of $\text{Li}_{0.3-0.5x}\text{Zn}_{0.4}\text{Ca}_x\text{Fe}_{2.3-0.5x}\text{O}_4$

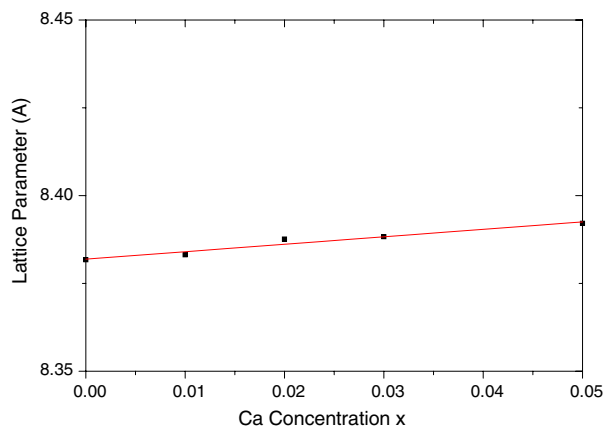


Fig. 2 The variation of the lattice parameter (Å) with Ca-concentration (x)

higher fields. The saturation magnetization M_s for each sample was determined by extrapolation of the magnetization curve to $H = 0$. The dependence of (M_s) on the Ca-concentration (x) is shown in Fig. 4. It is noticed that M_s increases rapidly with x and attains a maximum value at $x = 0.01$. Further increase of Ca-concentration leads M_s to decrease. Such a result could be discussed assuming the following cation distribution:



where the brackets () and [] denote A- and B-sites, respectively. Such cation distribution is based on the following facts:

1. Li^{1+} ions have a strong preference to occupy the B-site (Ref 7) while Zn^{2+} ions have a strong preference to occupy the A-site (Ref 8).
2. As for Ca-ion distribution, it was reported that Ca^{2+} ions strongly prefer to occupy the A-site for low Ca-concentration (Ref 6, 9). However, for high Ca-concentration, it was suggested that the Ca^{2+} ions are either distributed between A- and B-sites (Ref 10) or reside at the grain boundaries (Ref 11). Thus, according to the assumed cation distribution (Ca ions occupy the A-sites) increasing

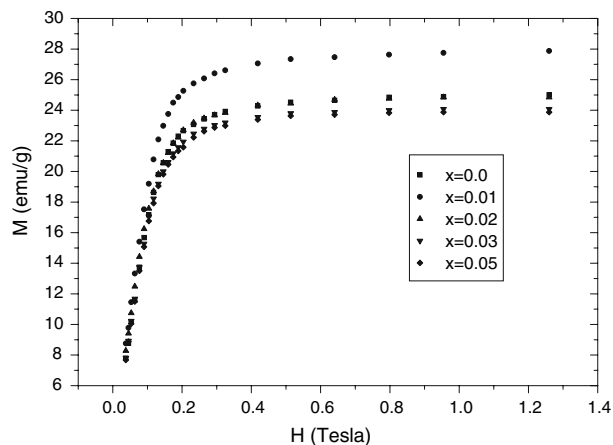


Fig. 3 The magnetization (emu/g) vs. the applied magnetic field H (T)

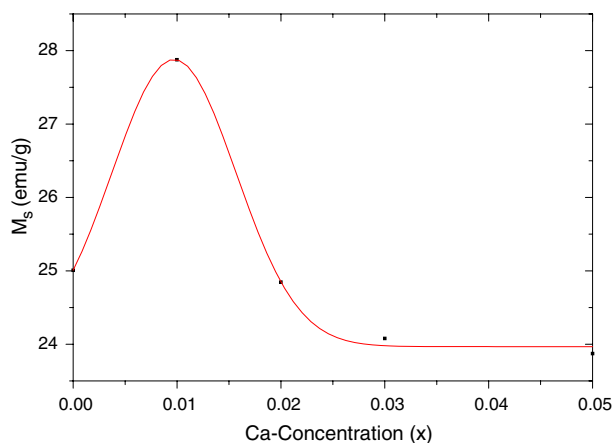


Fig. 4 The variation of saturation magnetization M_s (emu/g) with Ca-concentration (x)

of the Ca-concentration from $x = 0$ to $x = 0.01$ leads Fe^{3+} content in B-site to increase and that in A-site to decrease. Hence the total magnetization ($M_s = M_B - M_A$) increases. For $x > 0.01$, more Fe^{3+} ions migrate to B-site causing the B-B interaction to increase and hence the canting angle (θ_{YK}) establishes. It is expected that (θ_{YK}) increases with increasing Ca-concentration. Such an increase in (θ_{YK}) leads to a decrease of M_s according to the equation (Ref 12) $M_s = M_B \cos \theta_{\text{YK}} - M_A$, where M_A and M_B are the magnetizations of A- and B-sites, respectively. Thus our results support the occupation of Ca ions for A-sites at low Ca-concentration.

4.2 Initial Permeability

Figure 5 shows the variation of the initial permeability μ_i with temperature for the series $\text{Li}_{0.3-0.5x}\text{Zn}_{0.4}\text{Ca}_x\text{Fe}_{2.3-0.5x}\text{O}_4$ ($x = 0.0, 0.01, 0.02, 0.03, \text{ and } 0.05$). It is seen that the initial permeability increases with temperature up to Curie temperature T_c . Near T_c there is a sharp drop in μ_i . This result could be explained according to the Globus relation (Ref 13), which is given by

$$\mu_i \propto (M_s^2 D / K_1^{1/2})$$

where D is the average grain size and K_1 is the anisotropy constant. According to the Globus relation, the dependence of μ_i on temperature results from the temperature dependence of M_s and K_1 . It is known that the anisotropy field usually decreases much faster with temperature than M_s (Ref 14) which leads to an increase in μ_i . Figure 5 shows also that the rate of increase of μ_i with temperature decreases by increasing Ca-content. This may lead us to conclude that the Ca^{2+} ions improve the thermal stability of μ_i for the investigated samples (Ref 14) by compensating changes in M_s and K_1 with temperature. The compensating mechanism is still under investigation.

Furthermore, from Fig. 5 one can conclude that μ_i , at room temperature, decreases with increasing Ca-concentration. This is illustrated in Fig. 6 in addition to the variation of the porosity with Ca content. It is obvious that as the porosity increases, μ_i

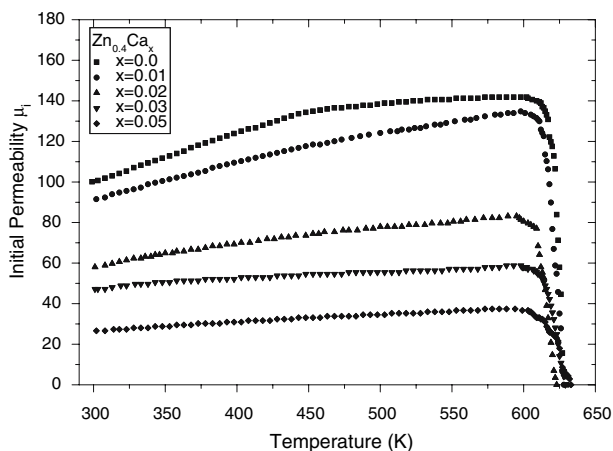


Fig. 5 The temperature dependence of the initial permeability μ_i for different Ca-concentrations (x)

decreases with increasing Ca-concentration. The decrease of μ_i with increasing x could be discussed using Globus relation as follows.

According to the proposed cation distribution, the amount of iron in B-site increases, which in turn increases the amount of Fe^{2+} in B-site. According to the one ion model, the anisotropy constant K_1 has a direct relation with the amount of Fe^{2+} . Therefore, as Ca-concentration increases, K_1 also increases. Furthermore, previous studies (Ref 1) have shown that doping Li-Zn ferrite with CaO decreases the grain size D . These two factors and the increase in porosity lead to the decrease of μ_i with increasing x . Moreover, the decrease of M_s in the range $0.01 < x \leq 0.05$, may contribute in decreasing μ_i .

5. Curie Temperature

The values of Curie temperature (T_c) were determined from the extrapolation of the linear part at the sudden decrease of μ_i of Fig. 5 for all investigated samples. The values of T_c and the rate of decrease of μ_i (slope of the linear part) are given in Table 1.

Table 1 illustrates that T_c is almost constant (628 ± 5 K). The constancy of T_c is discussed as follows. It is known that, in ferrites, T_c depends mainly on the A-B interaction, which in turn is affected by the following factors:

1. The magnitude and the concentration of magnetic moments existed in A- and B-sites. In our investigated system, the only moments existed those of Fe^{3+} ion. Moreover, the relative concentration of the moments on

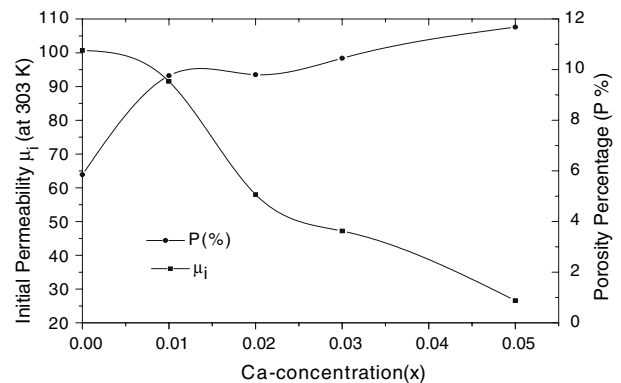


Fig. 6 The variation of the initial permeability μ_i , at room temperature, and porosity P (%) with Ca-concentration (x)

Table 1 The values of T_c (K) and rate of decrease of μ_i with Ca-concentration

Ca-Conc. (x)	T_c (K)	Rate of decrease of μ_i
0.0	628	-15.85
0.01	628	-9.25
0.02	623	-5.56
0.03	630	-3.97
0.05	633	-2.07

A- and B-sites (M_A/M_B) is almost constant, where for unsubstituted sample (M_A/M_B) = 0.353, and for the highest substituted sample (M_A/M_B) = 0.319.

- The distance between the A- and the B-sites where Fig. 2 shows that the change of lattice parameter with Ca-concentration, 0.025 Å/Ca content, is very small to affect $T_{c,o}$

Thus, according to the above factors, T_c tends to be almost constant which we have found experimentally.

Table 1 indicates also that the slope of the linear part of $\mu_i(T)$ curve, at the sudden decrease of μ_i , decreases with increasing Ca^{2+} concentration. It was reported that the value of this slope gives a good indication about the sample homogeneity (Ref 15), the higher the slope the higher the homogeneity. Thus one concludes that the homogeneity decreases with increasing Ca-concentration. Such a result could be attributed to the increase of the porosity with Ca-concentration.

6. Coercivity and Squareness

The variations of the coercive field H_c and the remanence ratio (B_r/B_s), which expresses the squareness of the hysteresis loop, for all Ca-concentrations (x) at a field $H = 340$ A/m are given in Table 2.

One can observe that H_c increases with increasing x . Similar results were reported by Rezlescu et al. (Ref 16) for Ni-Zn ferrite doped with CaO. Table 2 shows also that the ratio (B_r/B_s) increases with increasing Ca-concentration (x). These results are in agreement with that of the porosity. As the porosity increases, then higher field is needed to push the domain wall, i.e., H_c increases. Moreover, the behavior of M_s may play an indirect role in increasing H_c , specially for $x > 0.01$, through Brown's relation (Ref 17) which is given by

$$H_c \geq (2K_1/\mu_0 M_s)$$

Furthermore, it is known that the remanence B_r is directly proportional to the porosity (Ref 18). Moreover, for $x \leq 0.01$, the porosity increases by a factor of 67% while M_s increases only by a factor of 11.5%. This leads to an increase of B_r/B_s . In addition, for the range $0.01 < x \leq 0.05$, the porosity continues to increase while M_s decreases. This causes more increase of B_r/B_s .

6.1 Resistivity at Room Temperature

The dc resistivity (ρ) of all samples, at room temperature, are given in Table 3.

The table indicates that in the range $0 < x \leq 0.02$, the dc resistivity (ρ) decreases with increasing Ca-concentration (x), while ρ increases again for $x > 0.02$. This result could be explained as follows:

It was assumed above that the Ca^{2+} ions occupy the A-site for Ca-concentration up to $x = 0.01$. Hence, some Fe^{3+} ions migrate from A- to the B-site. The migration of Fe^{3+} is accompanied by the formation of Fe^{2+} ions in B-site (Ref 19). Thus the ratio of Fe^{2+}/Fe^{3+} ions in B-site increases. Thus the probability of hopping between Fe^{2+} and Fe^{3+} increases and hence, the resistivity decreases. For higher Ca-concentration, the effect of the porosity becomes the dominant factor and the resistivity increases.

Table 2 The values of H_c (A/m) and (B_r/B_s) with Ca-concentration (x)

Ca-Conc. (x)	H_c (A/m)	(B_r/B_s)
0.0	92	0.17
0.01	100	0.22
0.02	111	0.32
0.03	120	0.33
0.05	143	0.44

Table 3 The variations of ρ (Ω cm) with Ca-concentration

Ca-Conc. (x)	ρ (Ω cm) $\times 10^7$
0.0	3.6
0.01	0.1
0.02	0.08
0.03	2.1
0.05	30.4

7. Conclusion

Single spinel phases of Ca-substituted Li-Zn ferrite are studied. The Ca-substitution slightly increased the lattice parameter, the coercivity and the squareness of the samples. The magnetization increased for small Ca-concentration, $x = 0.01$, and then decreased for higher Ca content. The homogeneity of the samples and initial permeability decreased with increasing Ca-concentration while Curie temperatures are found to be almost constant.

References

- N. Rezlescu and E. Rezlescu, The Influence of Additives on the Material Parameters of Li-Zn Ferrites, *Phys. Stat. Sol. (a)*, 1995, **147**, p 553–562 (in English)
- H.T. Kim and H.B. Im, Effects of Bi_2O_3 and Nb_2O_5 on the Magnetic Properties of Ni-Zn Ferrites and Lithium Ferrites, *IEEE Trans. Magn.*, 1982, **18**(6), p 1541–1543 (in English)
- E. Bermejo, T. le Mercier, and M. Quarton, Microstructure and Physicochemical Studies of Pure and Zinc-Substituted Lithium Ferrites Sintered Above 1000°C, *J. Am. Ceram. Soc.*, 1995, **78**(2), p 365–368 (in English)
- S.A.J. Poltinnikov, Some Magnetic Properties of Nickel-Cadmium Ferrite, *Sov. Phys. Solid Stat.*, 1966, **8**, p 1144–1149 (in English)
- B.D. Cullity, *Elements of X-ray Diffraction*, Second printing, Addison-Wesley Publishing Company, Inc, USA, 1959
- N. Rezlescu and E. Rezlescu, Effects of Addition of Na_2O , Sb_2O_3 , CaO , and ZrO_2 on the Properties of Lithium Zinc Ferrite, *J. Am. Ceram. Soc.*, 1996, **79**(8), p 2105–2108 (in English)
- G.O. White and C.E. Patton, Magnetic Properties of Lithium Ferrite Microwave Materials, *J. Magn. Magn. Mater.*, 1978, **9**, p 299–317 (in English)
- Z.C. Xu, Magnetic Anisotropy and Mössbauer Spectra in Disordered Lithium-Zinc Ferrites, *J. Appl. Phys.*, 2003, **93**(8), p 4746–4749 (in English)
- R.V. Upadhyay, G.J. Baldha, and R.G. Kulkarni, Mössbauer study of the $Ca_xCo_{1-x}Fe_2O_4$ system, *J. Magn. Magn. Mater.*, 1986, **61**, p 109–113 (in English)
- S.D. Chhaya, M.P. Pandya, M.C. Chhantbar, K.B. Modi, G.J. Baldha, and H.H. Joshi, Study of Substitution Limit, Structural, Bulk Magnetic

- and Electrical Properties of Ca^{2+} Substituted Magnesium Ferrite, *J. Alloys Comp.*, 2004, **377**, p 155–161 (in English)
11. A.Y. Lipare, P.N. Vasambekar, and A.S. Vaingankar, Ac Susceptibility Study of CaCl_2 Doped Copper–Zinc Ferrite System, *Bull. Mater. Sci.*, 2003, **26**(5), p 493–497 (in English)
 12. S.S. Suryawanshi, V.V. Deshpande, U.B. Deshmukh, S.M. Kabur, N.D. Chaudhari, and S.R. Sawant, XRD Analysis and Bulk Magnetic Properties of Al^{3+} Substituted Cu–Cd Ferrites, *Mater. Chem. Phys.*, 1999, **59**, p 199–203 (in English)
 13. G.C. Jain, B.K. Das, R.S. Khanduja, and S.C. Gupta, Effect of Intragranular Porosity of Initial Permeability and Coercive Force in a Manganese Zinc Ferrite, *J. Mater. Sci.*, 1976, **11**, p 1335–1338 (in English)
 14. A.M. Sankpal, S.V. Kakatkar, N.D. Chaudhari, R.S. Patil, S.R. Sawant, and S.S. Suryavanshi, Initial Permeability Studies on Al^{3+} and Cr^{3+} Substituted Ni–Zn Ferrites, *J. Mater. Sci. Mater. Electron.*, 1998, **9**, p 173–179 (in English)
 15. A. Globus, H. Pascard, and V.J. Cagan, Distance Between Magnetic Ions and Fundamental Properties in Ferrites, *J. De Phys. Colloque*, 1977, **38**(4), p C1-163–C1168 (in English)
 16. E. Rezlescu, N. Rezlescu, C. Pasnicu, M.L. Craus, and D.D. Popa, The Influence of Additives on the Properties of Ni–Zn Ferrite Used in Magnetic Heads, *J. Magn. Magn. Mater.*, 1992, **117**, p 448–454 (in English)
 17. J.M.D. Coey, *Rare Earth Permanent Magnetism*. 1st ed., John Wiley and Sons, New York, 1996, 220
 18. R.M. Bozorth, *Ferromagnetism*. 7th ed., Van Nostrand Company, Inc, Princeton, New Jersey, 1963, 824
 19. N. Miyata, Electric Conduction of Ferrites Containing Fe^{2+} -ions, *J. Phys. Soc. (Jpn)*, 1961, **16**, p 206–208 (in English)